Calculation of minority-carrier mobilities in heavily doped *p*-type semiconductors in the dielectric-function formalism

T. Kaneto,* K. W. Kim, and M. A. Littlejohn
Department of Electrical and Computer Engineering, North Carolina State University, Raleigh, North Carolina 27695-7911
(Received 19 May 1992; revised manuscript received 19 February 1993)

An alternative approach for the calculation of minority-carrier mobilities is proposed. This approach is based on the self-consistent-field (SCF) method, and it combines elementary excitation theory with an appropriate transport theory beyond the relaxation-time approximation. Detailed information on elementary excitations of majority holes at *finite* temperature is obtained from the spectral density function ($\mathrm{Im}[-1/\varepsilon(q,\omega)]$) derived by the SCF method. Also, the *finite* lifetime of holes has been incorporated and a suitable form for the coupling of longitudinal-optical phonons, plasmons, and single-particle excitations is described. We have calculated minority-carrier mobilities for *p*-type GaAs and *p*-type Si, which show excellent agreement with available experimental data for a wide range of hole concentrations. Suggestions for improvements to this approach are described.

I. INTRODUCTION

Minority electron mobility in heavily-doped semiconductors is an important macroscopic quantity in many applications and several issues concerning this physical property of semiconductors remain to be resolved. Evaluation of minority-carrier mobility is a nontrivial problem, both experimentally and theoretically. Increasing data for minority electron mobility have become available in recent years, especially for GaAs. These data have been obtained from sophisticated experiments such as the time-of-flight measurement[1-5] and the common-emitter cutoff frequency measurement with adequately fabricated heterojunction bipolar devices,[6-8] in addition to other experimental methods.[9-11] Experiments for Si are fewer in number.[12-14]

Theoretical calculations of the minority electron mobility for GaAs were first made by the variational method.[15] Recently, Monte Carlo simulations have also been applied.[16-18] However, as pointed out by Beyzavi *et al.*, the calculated mobility does not agree well with their experimental data, either at room temperature or at low temperature.[8] At room temperature, the observed minority electron mobility is as much as a factor of 2 below the ionized impurity-dominated value. As temperature decreases, the experimental mobility increases much more sharply than the theoretical prediction. The variational method and Monte Carlo simulations are both effective for the calculation of carrier mobilities when the scattering mechanisms are described correctly. In earlier theories, electron-hole scattering was calculated by the same formula as that used for ionized impurity scattering in the center-of-mass coordinate system, and plasmon scattering was neglected. This approximation loses validity for fully degenerate conditions since hole transitions are strongly prohibited by the Pauli exclusion principle, while the collective excitation (i.e., plasmon) comes into play.

Minority electron transport should be described by the appropriate application of the many-body theory. The significant many-body effects are dynamical screening and collective excitations. Very recently, Lowney and Bennett showed a refined calculation of majority- and minority-carrier mobilities for GaAs (Ref. 19) and Si.[20] They incorporated plasmon scattering in the variational method, and applied phase-shift corrections beyond the Born approximation for ionized impurity scattering and minority-carrier–majority-carrier scattering, where the Pauli exclusion principle for majority carriers was approximated by removing those states with energies below the Fermi energy. Also, Fischetti reported a detailed study of the effects of plasmon scattering on the majority- and minority-carrier mobilities along with a phase-shift analysis for ionized impurity scattering in Si.[21] In these calculations, the effects of interband transition of holes were neglected and the Bohm and Pines approach of introducing a wave-vector cutoff[22] was adopted for the electron-hole interaction. As pointed out by Rorison and Herbert in their study of the electron-electron interaction using the random-phase approximation (RPA), the concept of wave-vector cutoff in *n*-type semiconductors becomes invalid as the carrier density is lowered.[23] In heavily-doped *p*-type semiconductors, the definition of a cutoff wave vector for hole plasmons becomes more ambiguous due to the extended and complicated Landau damping region. The dynamical response of a hole gas is significantly affected by interband transitions between the heavy-hole band and the light-hole band.[24,25] In addition, our recent work[26] has demonstrated the importance of collision damping of coupled collective excitations due to finite hole lifetime, i.e., the short interval time between scattering events. The resulting damped plasma modes are coupled to longitudinal-optical (LO) phonons in zinc-blende semiconductors. Coupling of hole-plasmon–LO-phonon modes and the broadening of these modes in *p*-type GaAs have been observed experimentally by Raman scattering.[27-29] Major issues which need to be addressed in minority electron mobility calculations include (i) electron-hole interactions related to the interband hole transitions within the valence bands and (ii) the

coupling of LO phonons and plasmons.

An effective method to describe minority-carrier transport in a heavily-doped semiconductor is to extend the dielectric-response-function formalism to an appropriate transport theory. Although there are limitations, the RPA or self-consistent-field (SCF) method is a tractable and reasonable approach for describing the many-body effects in heavily-doped semiconductors since the effective interparticle radius is usually small in such materials.[30] By evaluating the frequency- and wave-vector-dependent dielectric-response functions for majority holes, we can develop a more comprehensive method for the calculation of minority electron transport. In this method, detailed information of elementary excitations of the hole gas is obtained from the spectral density function ($\mathrm{Im}[-1/\varepsilon(q,\omega)]$), and the static dielectric function $\varepsilon(q,0)$ describes the screened impurity potential incorporating the multiple structure of the valence band.

The purpose of this paper is to examine the accuracy of our dielectric-function approach derived by the combination of elementary excitation theory and an appropriate transport theory. Our model incorporates the dynamical interaction between minority electrons and majority holes within the Born approximation. The calculated results are compared with experimental data for heavily-doped p-type GaAs and Si.

II. THEORY

A. Basic formulas

In order to describe inelastic scattering correctly, we adopt the iterative method[31] since the relaxation-time approximation cannot be applied when nonrandomizing inelastic-scattering mechanisms dominate. Under weak-field conditions, we can apply the first-order Legendre polynomial expansion of the full distribution function,

$$f(\mathbf{k})=f_0(E_\mathbf{k})-eFv(\mathbf{k})\phi(E_\mathbf{k})\frac{\partial f_0(E_\mathbf{k})}{\partial E_\mathbf{k}}\cos\theta\ , \tag{1}$$

where θ is the angle between velocity $\mathbf{v}(\mathbf{k})$ and electric field $\mathbf{F}$. Here, we assume a spherical conduction band incorporating first-order nonparabolicity, i.e., the energy-momentum relation is given by

$$\frac{\hbar^2k^2}{2m^*}=\gamma(E_\mathbf{k})=E_\mathbf{k}(1+\alpha E_\mathbf{k})\ , \tag{2}$$

where m^* is the effective mass at the bottom of the conduction band. The nonparabolicity factor α has a moderate effect on mobility at room temperature. The electron velocity is given by

$$\mathbf{v}(\mathbf{k})=\frac{\hbar\mathbf{k}}{m^*(1+2\alpha E_\mathbf{k})}\ . \tag{3}$$

We assume nondegenerate statistics for minority-carrier distribution. Thus, the iterative form for $\phi(E_\mathbf{k})$ in our case is given by

$$\phi(E_\mathbf{k})=\frac{1+\Gamma(\phi,E_\mathbf{k})}{1/\tau(E_\mathbf{k})+\Gamma_0(E_\mathbf{k})}\ , \tag{4}$$

where $\tau(E_\mathbf{k})$ is the relaxation time for elastic scattering,

$$\frac{1}{\tau(E_\mathbf{k})}=\frac{1}{8\pi^3}\int W^{\mathrm{el}}_{\mathbf{k},\mathbf{k}'}[1-\cos\Theta]d\mathbf{k}'\ . \tag{5}$$

Here, $W^{\mathrm{el}}_{\mathbf{k},\mathbf{k}'}$ is the elastic-scattering rate from $\mathbf{k}$ to $\mathbf{k}'$ and Θ is the angle between $\mathbf{k}$ and $\mathbf{k}'$. Also, $\Gamma_0(E_\mathbf{k})$ and $\Gamma(\phi,E_\mathbf{k})$ are defined by the following integrals:

$$\Gamma_0(E_\mathbf{k})=\frac{1}{8\pi^3}\int W^{\mathrm{in}}_{\mathbf{k},\mathbf{k}'}d\mathbf{k}'\ , \tag{6}$$

$$\Gamma(\phi,E_\mathbf{k})=\frac{1}{8\pi^3}\int W^{\mathrm{in}}_{\mathbf{k},\mathbf{k}'}\phi(E_{\mathbf{k}'})\frac{\mathbf{v}(\mathbf{k}')}{\mathbf{v}(\mathbf{k})}\cos\Theta d\mathbf{k}'\ . \tag{7}$$

Here, $W^{\mathrm{in}}_{\mathbf{k},\mathbf{k}'}$ is the inelastic-scattering rate from $\mathbf{k}$ to $\mathbf{k}'$; thus, $\Gamma_0(E_\mathbf{k})$ is the total inelastic-scattering rate. Retaining first-order nonparabolicity, we obtain the minority-carrier mobility as

$$\mu=\frac{2e}{3k_BTm^*}\times\frac{\int_0^\infty\phi(E_\mathbf{k})E_\mathbf{k}^{3/2}(1-\frac{1}{2}\alpha E_\mathbf{k})\exp(-E_\mathbf{k}/k_BT)dE_\mathbf{k}}{\int_0^\infty E_\mathbf{k}^{1/2}(1+\frac{5}{2}\alpha E_\mathbf{k})\exp(-E_\mathbf{k}/k_BT)dE_\mathbf{k}}\ . \tag{8}$$

B. Scattering mechanisms in zinc-blende semiconductors

In heavily-doped zinc-blende semiconductors (e.g., GaAs), the dominant scattering mechanisms are ionized impurity scattering and inelastic scattering due to the coupled LO-phonon-plasmon excitation and the single-hole excitation. The elastic-scattering rate due to ionized impurities is given in the Born approximation by

$$W^{\mathrm{el}}_{\mathbf{k},\mathbf{k}+\mathbf{q}}=N_i\frac{2\pi}{\hbar}|\langle\mathbf{k}+\mathbf{q}|V(\mathbf{r})|\mathbf{k}\rangle|^2\delta(E_{\mathbf{k}+\mathbf{q}}-E_\mathbf{k})\ , \tag{9}$$

$$V(\mathbf{r})=\sum_\mathbf{q}\frac{4\pi e^2}{\varepsilon(q,0)q^2}e^{i\mathbf{q}\cdot\mathbf{r}}\ , \tag{10}$$

where $\varepsilon(q,0)$ is the SCF static dielectric function and N_i is the density of ionized impurities. The SCF method is a good approximation since the SCF dielectric function can incorporate the anisotropic band structure and reproduce characteristic features of the potentials obtained by the nonlinear Hartree approximation and the Kohn-Sham approximation.[32] We assume that the compensation ratio is zero and that all of the acceptor impurities are ionized, i.e., $p=N_i$. This assumption eliminates the use of some fitting parameters. The final form for evaluation of the relaxation time for elastic scattering is

$$\frac{1}{\tau(E_{\mathbf{k}})}=\frac{1}{\tau_{\rm imp}(E_{\mathbf{k}})}=\frac{4\pi N_i e^2 m^*(1+2\alpha E_{\mathbf{k}})}{\hbar^3 k^3}\times\int_0^1\frac{d\eta}{\eta[\varepsilon(2k\eta,0)]^2}\ , \tag{11}$$

where $\eta=\sin\Theta/2$.

The inelastic-scattering rate is given by the spectral density function {i.e., $\mathrm{Im}[-1/\varepsilon(q,\omega)]$} in the Born approximation,[33]

$$W^{\rm in}_{\mathbf{k},\mathbf{k}+\mathbf{q}}=\int d(\hbar\omega)\frac{2\pi}{\hbar}\frac{4e^2}{q^2}\mathrm{Im}\left[-\frac{1}{\varepsilon(q,\omega)}\right][1+n(\hbar\omega)]\times\delta(E_{\mathbf{k}+\mathbf{q}}-E_{\mathbf{k}}+\hbar\omega)\ . \tag{12}$$

Using Eqs. (6) and (7) we obtain

$$\Gamma_0(E_{\mathbf{k}})=\frac{2e^2m^*}{\pi\hbar^3k}\int_0^\infty\frac{dq}{q}\int_{\hbar\omega_{\min}}^{\hbar\omega_{\max}}d(\hbar\omega)\mathrm{Im}\left[-\frac{1}{\varepsilon(q,\omega)}\right][1+n(\hbar\omega)][1+2\alpha(E_{\mathbf{k}}-\hbar\omega)]\ , \tag{13}$$

$$\Gamma(\phi,E_{\mathbf{k}})=\frac{2e^2m^*(1+2\alpha E_{\mathbf{k}})}{\pi\hbar^3k}\int_0^\infty\frac{dq}{q}\int_{\hbar\omega_{\min}}^{\hbar\omega_{\max}}d(\hbar\omega)\phi(E_{\mathbf{k}}-\hbar\omega)\left[1-\frac{q^2}{2k^2}-\frac{\gamma(E_{\mathbf{k}})-\gamma(E_{\mathbf{k}}-\hbar\omega)}{2\gamma(E_{\mathbf{k}})}\right]\times\mathrm{Im}\left[-\frac{1}{\varepsilon(q,\omega)}\right][1+n(\hbar\omega)]\ , \tag{14}$$

where $n(\hbar\omega)$ is the Bose function and $\gamma(E_{\mathbf{k}})$ is defined by Eq. (2). The limits of integration are taken as $\hbar\omega_{\max}=\hbar^2q(2k-q)/2m^*(1+2\alpha E_{\mathbf{k}})$, $\hbar\omega_{\min}=\max\{-\hbar^2q(2k+q)/2m^*(1+2\alpha E_{\mathbf{k}}),\ -6k_BT\}$, and $0<q<k+[k^2+12k_BTm^*(1+2\alpha E_{\mathbf{k}})/\hbar^2]^{1/2}$. These expressions imply both energy emission and absorption processes. The dielectric-response function for a zinc-blende semiconductor is calculated from the following equation:[26,34]

$$\varepsilon(q,\omega)=\varepsilon_\infty-\frac{4\pi e^2}{q^2}\frac{(1+i/\omega\tau_h)P(q,\omega+i/\tau_h)}{1+(i/\omega\tau_h)P(q,\omega+i/\tau_h)/P(q,0)}+\frac{\varepsilon_\infty(\omega_{\rm LO}^2-\omega_{\rm TO}^2)}{\omega_{\rm TO}^2-\omega^2-i\omega\Gamma_T} \tag{15}$$

where ε_∞ is the high-frequency dielectric constant, and $\omega_{\rm LO}$ ($\omega_{\rm TO}$) is the longitudinal- (transverse-) optical phonon frequency. The second term in Eq. (15) is the hole dielectric function derived by the SCF approach, where $P(q,\omega+i/\tau_h)$ is given by

$$P(q,\omega+i/\tau_h)=\sum_{n,l}\sum_{\mathbf{k}}|F^{\mathbf{k},\mathbf{k}+\mathbf{q}}_{n,l}|^2\left[\frac{f_l(\mathbf{k}+\mathbf{q})-f_n(\mathbf{k})}{E_l(\mathbf{k}+\mathbf{q})-E_n(\mathbf{k})-\hbar(\omega+i/\tau_h)}\right] \tag{16}$$

For the valence bands in zinc-blende semiconductors, the overlap factor is given by[24]

$$|F^{\mathbf{k},\mathbf{k}+\mathbf{q}}_{n,l}|^2=\begin{cases}1-\dfrac{3q^2\sin\varphi}{4|\mathbf{k}+\mathbf{q}|^2}\ , & n=l\\ \dfrac{3q^2\sin^2\varphi}{4|\mathbf{k}+\mathbf{q}|^2}\ , & n\neq l\end{cases} \tag{17}$$

where the indices n and l denote either the heavy-hole band or the light-hole band, and φ is the angle between $\mathbf{k}$ and $\mathbf{q}$. The hole relaxation time τ_h (not to be confused with the electron relaxation time τ) is obtained from the experimental hole mobility (i.e., $1/\tau_h=e/\mu_h m_h$). The third term in Eq. (15) is the lattice dielectric function and Γ_T is the damping constant due to the anharmonicity of optical phonons.

C. Scattering mechanisms in covalent semiconductors

For heavily-doped covalent semiconductors (e.g., Si), the dominant scattering mechanisms are almost the same as for zinc-blende semiconductors with some modification. Since there is no polar optical interaction in covalent semiconductors, the total dielectric-response function is given by

$$\varepsilon(q,\omega)=\varepsilon_0-\frac{4\pi e^2}{q^2}\frac{(1+i/\omega\tau_h)P(q,\omega+i/\tau_h)}{1+(i/\omega\tau_h)P(q,\omega+i/\tau_h)/P(q,0)}\ , \tag{18}$$

where ε_0 is the static dielectric constant. In the spherical band approximation, we can use the same formulas given by Eqs. (11), (13), and (14).

In addition to the above scattering processes, we consider acoustic-phonon scattering and intervalley phonon scattering. Screening for the deformation potential is an unsolved problem since the "unscreened potential" cannot be defined explicitly in the presence of free carriers.[35,36] However, if we assume that nuclear displacement produced by the phonons is the same in the absence or presence of free carriers (although this is not true in general), the deformation potential is screened by free carriers in exactly the same way as the macroscopic potentials from long-range interactions.[36] In this assumption, for consistency, we incorporate screening for acoustic-phonon scattering using the SCF dielectric func-

tion. Since the phonon energy is much smaller than the thermal energy, we can assume energy equipartition, the elastic-scattering approximation, and the static screening approximation. Dividing the q-Fourier component of the unscreened deformation potential by $[\varepsilon(q,0)/\varepsilon_0]$, we obtain the scattering rate of an electron from $\mathbf{k}$ to $\mathbf{k}+\mathbf{q}$,

$$W^{\rm ac}_{\mathbf{k},\mathbf{k}+\mathbf{q}}=\frac{2\pi k_B T\Xi^2}{\hbar u^2\rho}\left[\frac{\varepsilon_0}{\varepsilon(q,0)}\right]^2\delta(E_{\mathbf{k}+\mathbf{q}}-E_{\mathbf{k}})\ , \tag{19}$$

where Ξ is the deformation-potential constant, u is the longitudinal sound velocity, and ρ is the density of the material. Thus, unlike the unscreened potential, acoustic-phonon scattering becomes anisotropic for momentum relaxation when screening is included. The final form of the relaxation time [Eq. (5)] is then given by

$$\frac{1}{\tau_{\rm ac}(E_{\mathbf{k}})}=\frac{2^{5/2}m^{*3/2}k_B T\Xi^2}{\pi\hbar^4u^2\rho}E_{\mathbf{k}}^{1/2}(1+\tfrac{5}{2}\alpha E_{\mathbf{k}})\times\int_0^1\left[\frac{\varepsilon_0}{\varepsilon(2k\eta,0)}\right]^2\eta^3d\eta\ . \tag{20}$$

On the other hand, screening of intervalley phonon scattering can be neglected since intervalley scattering is accompanied by a large momentum transfer [$\varepsilon(q,\omega)\rightarrow\varepsilon_0$ when $q\rightarrow+\infty$]. Also, although intervalley phonon scattering is an inelastic process, Γ given by Eq. (7) becomes zero since the intervalley phonon scattering is a momentum randomizing process for final states.[31] Therefore, we can define a "relaxation time" for this scattering as[37]

$$\frac{1}{\tau_{{\rm inter},i}(E_{\mathbf{k}})}\equiv\Gamma^{\rm inter}_{0,i}(E_{\mathbf{k}})=\frac{(D_tK)_i^2m^{*3/2}Z_f}{2^{1/2}\pi\hbar^3\rho\omega_i}\begin{bmatrix}n(\hbar\omega_i)\\ n(\hbar\omega_i)+1\end{bmatrix}\times\gamma^{1/2}(E_{\mathbf{k}}\pm\hbar\omega_i)\times[1+2\alpha(E_{\mathbf{k}}\pm\hbar\omega_i)]\ , \tag{21}$$

where $(D_tK)_i$ is the coupling constant, ω_i is the phonon frequency for ith phonon modes, and Z_f is the number of possible equivalent valleys. In both Eqs. (20) and (21), we use the material parameters listed in Ref. 37. Finally, the total relaxation time is then given by

$$\frac{1}{\tau(E_{\mathbf{k}})}=\frac{1}{\tau_{\rm imp}(E_{\mathbf{k}})}+\frac{1}{\tau_{\rm ac}(E_{\mathbf{k}})}+\sum_i\frac{1}{\tau_{{\rm inter},i}(E_{\mathbf{k}})}\ . \tag{22}$$

III. RESULTS AND DISCUSSION

A. Parameters

We have adopted the standard input parameters listed in Table I. However, the valence-band parameters require more careful consideration. In order to calculate Eq. (16), the parabolic band approximation for the valence band must be applied, although the actual valence band is quite complicated. In order to investigate the energy dependence of hole effective-mass ratios, which are assumed to be single values in our formalism, we have estimated "average conductivity effective-mass ratios" according to Ref. 38 as shown in Appendix A.

Figure 1 shows the average conductivity effective-mass ratios for holes as a function of hole energy in GaAs and Si. Here, we have adopted the valence-band parameters $A=-7.65$, $B=-4.82$, $C=-7.71$, and $\Delta=0.34$ eV for GaAs, with $A=-4.22$, $B=-0.78$, $C=-4.80$, and $\Delta=0.044$ eV for Si, where A, B, and C are given in atomic units.[39] As can be seen, the energy dependence of the valence-band effective-mass ratios is not significant for GaAs. Therefore, we have adopted the standard effective-mass values at the top of the valence bands reported in the literature. On the other hand, the nonparabolicity of the valence bands is quite significant for Si, producing important effects for very heavily-doped conditions. The strong dependence of hole effective-mass values on hole energy will influence the screening effects and collective excitations significantly. Larger effective-mass values will be more effective for static screening in the Coulomb interaction and produce smaller plasmon energy. In this paper, we have adopted two sets of effective-mass values as listed in Table I; the standard values at the top of the conduction band and the values deduced from Fig. 1. The latter choice is also consistent with the density-of-states effective-mass ratios for the large hole energy calculated in Ref. 40. We have also

TABLE I. Material parameters for GaAs and Si.

	GaAs	Si
Conduction-band parameters		
Conductivity effective-mass ratio	0.07	0.26
Density-of-states effective-mass ratio	0.07	0.32
Nonparabolicity factor (eV^{-1})	0.64	0.5
Valence-band parameters		
Heavy-hole effective-mass ratio	0.50	0.53(1.2[a])
Light-hole effective-mass ratio	0.082	0.155(0.2[a])
Dielectric parameters		
High-frequency dielectric constant	10.9	
Static dielectric constant		11.7
TO-phonon energy (meV)	33.8	
LO-phonon energy (meV)	36.5	

[a]Deduced from Fig. 1.

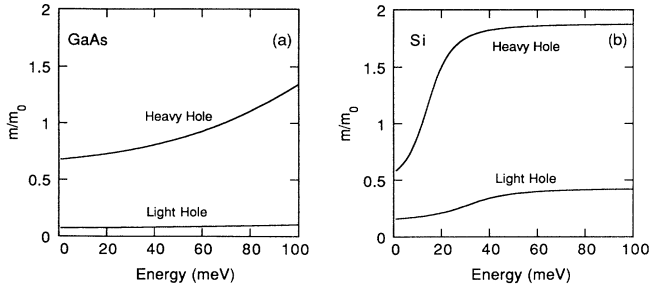

FIG. 1. Average conductivity effective-mass ratios for the valence bands in (a) GaAs and (b) Si obtained from the equations given in Appendix A.

neglected the split-off band. Although it is relatively close to the top of the valence band in Si, we assume the effect of the split-off band is small since its contribution to the total hole population is very small.

For the conduction band, we have assumed a single spherical band with first-order nonparabolicity. This approximation is fairly accurate for GaAs since most minority electrons are located near the bottom of the Γ valley at low electric field. For Si, we have used two effective-mass values for the conduction band, i.e., the conductivity effective mass ($m^*=m_c$) for mobility [Eq. (8)] and the density-of-states effective mass ($m^*=m_d$) for scattering rates [Eqs. (13), (14), and (22)].

Another important parameter in our theory is the damping constant $\hbar/\tau_h$ which is obtained from $1/\tau_h=e/\mu_h m_h$. For hole concentrations of interest, appropriate values of $\hbar/\tau_h$ are 0.01–0.05 eV since hole mobilities between 50 and 200 cm^2/V sec are typical for both GaAs and Si at room temperature. For the damping constant of optical phonons, we have adopted $\hbar\Gamma_T=2.5\times10^{-4}$ eV (≈2 cm^{-1}), which is the typical experimental value for GaAs at 300 K.[41]

B. Electron mobility in *p*-type GaAs

Our theoretical calculation has been compared in a quantitative way with experimental data for GaAs. The first test of the theory is the comparison of our results with experimental work of Beyzavi *et al.*, who investigated the temperature dependence of minority-carrier mobilities.[8] Figure 2 shows the temperature dependence of minority-carrier mobilities for a hole concentration of 4×10^{18} cm^{-3} with $\hbar/\tau_h$ as a parameter. We have assumed two values of $\hbar/\tau_h$ (0 and 0.02 eV) for comparison. Also plotted are the experimental data of Beyzavi *et al.* as well as the theoretical values obtained by the conventional method of Walukiewicz *et al.*[15] Our results show excellent agreement with the experimental data for $\hbar/\tau_h=0.02$ eV, which is obtained for a majority hole mobility of about 100 cm^2/V sec. The result with $\hbar/\tau_h=0$ gives systematically larger values than the experimental results. As shown in Fig. 2, the previous theory does not explain the temperature dependence of electron mobility,[8] where the electron-hole interaction was incorporated in the elastic-scattering approximation, i.e., "ionized impurity scattering" rates were merely doubled for uncompensated materials. This approximation may be qualitatively reasonable for a nondegenerate hole gas, since the hole mass is much larger than that of an electron and the scattered electron loses little energy during the scattering event. However, in a fully degenerate hole gas, most holes are prohibited from scattering due to the Pauli exclusion principle. This leads to a reduction of two-body scattering between a hole and an electron. This is the main reason why we observe a sharp increase in mobility as temperature decreases below about 150 K. At higher temperatures, on the other hand, two-body scattering is important and the collective excitations (hole plasmons, which are coupled to LO phonons in zinc-blende semiconductors) emerge as well, resulting in significant reduction of mobility.

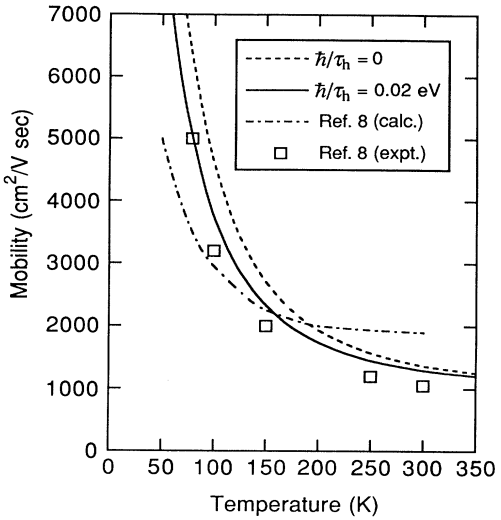

FIG. 2. Electron mobilities for GaAs as a function of temperature with $\hbar/\tau_h$ as a parameter (dashed line for $\hbar/\tau_h=0$ and solid line for $\hbar/\tau_h=0.02$ eV). The theoretical results are compared with the experimental data available in the literature, as well as the value calculated by the conventional method (dashed-dotted line).

In order to examine the scattering mechanisms more quantitatively, we have calculated the energy-dependent momentum relaxation rates. For this purpose, we define the "momentum relaxation rate" for inelastic scattering as

$$\frac{1}{\tau^{\rm in}(E_{\mathbf{k}})}=\int W^{\rm in}_{\mathbf{k},\mathbf{k}'}\left[1-\frac{\mathbf{v}(\mathbf{k}')}{\mathbf{v}(\mathbf{k})}\cos\Theta\right]d\mathbf{k}' , \tag{23}$$

where each symbol has the meaning described in Sec. II. This definition is sometimes used in the balance equations for solving transport problems and is also adopted in Ref. 21 for plasmon scattering. Although Eq. (23) is useful, e.g., for the evaluation of relaxation rates of hot electrons, it is strictly valid for the mobility calculation only when $\tau(E_{\mathbf{k}})=\tau(E_{\mathbf{k}'})$, as is the case for elastic scattering, where $\tau(E_{\mathbf{k}})$ is the total "momentum relaxation time." Therefore, if the total relaxation rates change abruptly with electron energy, this formula may give a significant

error in mobility calculations. Figure 3 shows the momentum relaxation rates for elastic and inelastic scattering obtained from Eq. (23) as a function of electron energy with $\hbar/\tau_h$ as a parameter at 77 K [Fig. 3(a)] and 300 K [Fig. 3(b)] for a hole concentration of 4×10^{18} cm^{-3}. For ionized impurity scattering, we have shown only one curve in each graph since the elastic-scattering rate is not affected by a finite value of τ_h.[26] In our formalism for inelastic scattering, for the sake of accuracy we do not distinguish LO-phonon scattering, plasmon scattering, and two-body scattering. At low temperature [Fig. 3(a) at 77 K], most electrons are located near the bottom of the conduction band [effective energy range in Eq. (8) is about 0–50 meV and the characteristic electron energy is $3k_BT/2\sim10$ meV], where the momentum relaxation rates due to inelastic scattering are increased by the finite value of τ_h. This is due to broadening of the collective excitation modes toward smaller ω at small q, which can interact with low-energy electrons. At higher temperature [Fig. 3(b) at 300 K], momentum relaxation rates due to both the elastic and inelastic scattering increase for low electron energy. Here, the increase of average hole energy results in weakening of static screening, and elementary excitations are thermally excited. Although the modification of the momentum relaxation rates for inelastic scattering due to the finite value of τ_h is significant, the actual effect on minority mobility is moderate at 300 K. Since the effective energy range in Eq. (8) is extended over about 0–150 meV, an increase in momentum relaxation rate at small electron energy and decrease at large electron energy cancel each other in the final result of mobility.

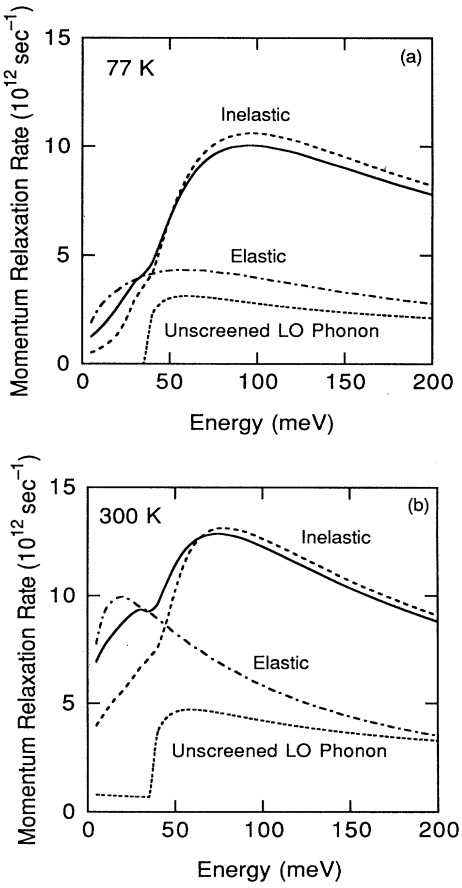

FIG. 3. Momentum relaxation rates $[1/\tau(E)]$ defined by Eq. (23) for minority electrons in GaAs as a function of electron energy for the ionized impurity scattering (dashed-dotted lines), and for total inelastic scattering with $\hbar/\tau_h$ as a parameter (dashed lines for $\hbar/\tau_h=0$ eV and solid lines for $\hbar/\tau_h=0.02$ eV) evaluated at (a) 77 K and (b) 300 K. The dotted lines denote the corresponding relaxation rates for unscreened LO-phonon scattering for comparison.

Figure 4 shows electron mobility at 300 K as a function of hole concentration with $\hbar/\tau_h$ as a parameter (solid line for $\hbar/\tau_h=0.02$ eV and dashed line for $\hbar/\tau_h=0.05$ eV), along with the experimental data from the literature. The dashed-dotted line is the result including the multi-ion screening correction, which will be discussed later. In general, as doping density becomes higher, hole mobility becomes smaller, resulting in a larger damping constant ($\hbar/\tau_h$). Although the experimental data are highly scattered, overall agreement is satisfactory, especially for hole concentration up to 10^{19} cm^{-3}. The tendency of the U-shaped curve qualitatively agrees with the results of Furuta and Tomizawa.[3] Near the minimum of the curve (around 3×10^{18} cm^{-3}), coupled collective excitations interact most effectively with thermally injected electrons. These features are clearly visible in Fig. 5, where momentum relaxation rates $[1/\tau(E_k)]$ are plotted for an electron energy of 40 meV ($\sim3k_BT/2$). The solid line, the dashed-dotted line, and the bold solid line denote momentum relaxation rates for inelastic scattering (calculated with $\hbar/\tau_h=0.02$ eV), elastic scattering, and the sum of these two, respectively. Also, the corresponding momentum relaxation rate due to unscreened LO-phonon scattering is shown (dotted line) for comparison. Up to the hole concentration of

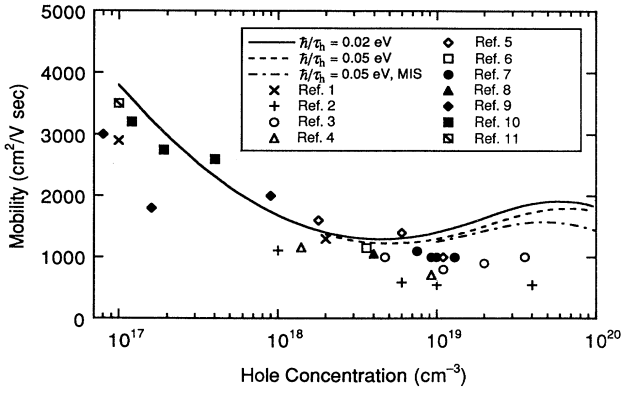

FIG. 4. Electron mobilities for GaAs as a function of hole concentration evaluated at 300 K with $\hbar/\tau_h$ as a parameter (solid line for $\hbar/\tau_h=0.02$ eV and dashed line for $\hbar/\tau_h=0.05$ eV). The theoretical values are compared with experimental data available in the literature. The dashed-dotted line denotes the results with multi-ion screening (MIS) correction.

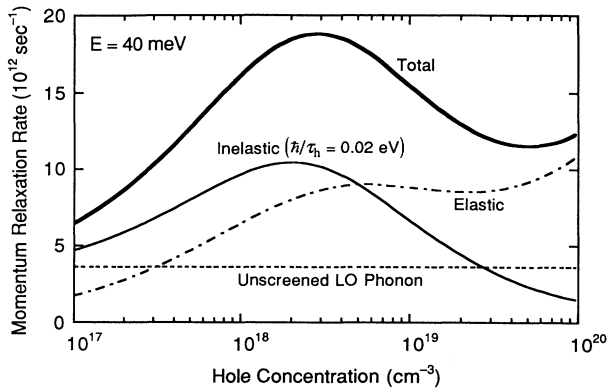

FIG. 5. Momentum relaxation rates in p-type GaAs for electron energy of 40 meV (which corresponds to $3/2k_BT$) at 300 K as a function of hole concentration. The solid line, dashed-dotted line, and bold solid line denote momentum relaxation rates due to inelastic scattering ($\hbar/\tau_h = 0.02$ eV), elastic scattering, and the sum of these two, respectively. The dotted line denotes the corresponding relaxation rates for unscreened LO-phonon scattering, as a reference.

about 3×10^{18} cm^{-3}, the LO phonon is antiscreened and the interaction with electrons is enhanced. At the same time, plasmon scattering is important. Antiscreening and screening for LO phonons in n-type zinc-blende semiconductors have been discussed by Ridley.[42] This condition ($p\sim3\times10^{18}$ cm^{-3}) is the coincidence point of the uncoupled LO phonon and the plasmon frequency, where actual two modes interact strongly. As hole concentration becomes larger than about 3×10^{18} cm^{-3}, the interaction between minority electrons and coupled modes becomes less effective and impurity scattering dominates. This is due to the fact that the plasmon energy becomes too large to interact with thermally injected electrons, and also the LO-phonon mode is strongly screened by higher-frequency plasmons. At very high hole concentrations, the momentum relaxation rates due to total inelastic scattering becomes even smaller than those for bare LO-phonon scattering. These effects result in an increase of minority-carrier mobilities for hole concentration above about 3×10^{18} cm^{-3} range. However, the mobility decreases again for the very heavily-doped conditions due to the increase of dominant impurity scattering rates.

In Fig. 4, the deviation of our results from experimental data becomes larger for the larger hole concentrations ($>10^{19}$ cm^{-3}), even when we adopt a larger collision damping constant (e.g., $\hbar/\tau_h = 0.05$ eV). In this regime, where ionized impurity scattering dominates with strong screening by majority holes, improvements in our theory are needed. For example, the Born approximation in our theory may not be adequate. The Born approximation for impurity scattering is accurate when $4k^2/q^2_{\rm TF}\gg1$ where k is the wave vector of an electron and $q_{\rm TF}$ is the Thomas-Fermi (or Debye-Huckel) screening vector.[43] Also, our basic assumption for inelastic scattering by collective excitations is that the electrons are weakly coupled to the many-particle system, which is true for *fast* electrons.[33] Thus, it may be essential in this regime (with the hole concentration greater than 10^{19} cm^{-3}) to go beyond the Born approximation, not only for ionized impurity scattering, but also for collective excitations. These issues have been discussed in a recent study using phase-shift analysis by Lowney and Bennett.[19] A rigorous and comprehensive treatment beyond the Born approximation is beyond the scope of this work. Here, an effort has been made to improve accuracy within the current formalism. We have applied the multi-ion current (MIS) correction for ionized impurity scattering discussed by Meyer and Bartoli[44] as shown in Appendix B, which is denoted by a dashed-dotted line in Fig. 4. This effect is significant in the strong screening limit. After incorporating the MIS correction, agreement with experimental values is improved although the difference is still about 30%. Other possible corrections include multiple scattering and impurity dressing discussed by Moore.[45] Although his final formula is easily applicable to our calculation and the effects may be significant, this theory is questionable since the truncation of the expansion after a few terms may be invalid even when the low-order terms are small.[44] Therefore, we have not adopted these corrections in this paper. We can also assume other possibilities from a practical point of view. The data appear to depend strongly on the experimental conditions, such as the species of dopants and the crystal quality of the material samples. The latest data by Colomb *et al.*[5] for samples with carbon doping give the highest values of mobility. On the other hand, the data by Keyes *et al.*[2] (doped with Mg and Zn) show systematically lower values than other experiments. The remaining data except for Refs. 9 and 10 (Ge doped) were obtained with Be-doped samples. Also, Furuta and Tomizawa[3] measured the high-field time of flight (>2.5 kV/cm), which results in more frequent scattering events than at low field. The high field strongly modifies the electron distribution and effective electron temperature, which would be better described by, e.g., the Monte Carlo method. However, evaluation of the field effect on screening is still an unsolved problem. Also, for very heavily-doped material, other effects such as the warped structure and band tailing of the valence band may become significant. For further discussion, more experimental data are needed. Unfortunately, experiments in this region are extremely difficult because of the very short recombination lifetime of minority carriers due to dominant Auger processes.

C. Electron mobility in p-type Si

Figure 6 shows minority-carrier mobility as a function of hole concentration calculated with two sets of hole effective-mass ratios. Here, we have assumed a single value of damping constant of $\hbar/\tau_h = 0.01$ eV. In our theory, the choice of appropriate hole effective-mass values is important and other corrections cause only secondary effects. The major differences of electron scattering mechanisms in Si from those in GaAs are the absence of the polar LO-phonon scattering and the contribution of other scattering mechanisms. Acoustic-

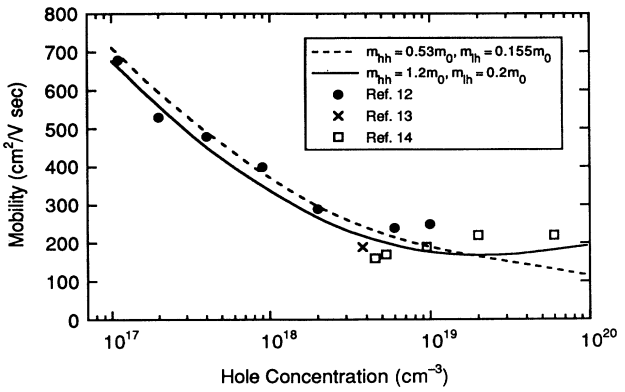

FIG. 6. Electron mobilities for Si as a function of hole concentration evaluated at 300 K with $\hbar/\tau_h = 0.01$ eV. The dashed line and the solid line are calculated with $m_{hh} = 0.53m_0$, $m_{lh} = 0.155m_0$, and $m_{hh} = 1.2m_0$, $m_{lh} = 0.2m_0$, respectively. The theoretical values are compared with experimental data available in the literature.

phonon scattering and intervalley phonon scattering play moderate roles in the reduction of mobility only at small doping densities although they can never be neglected. Screening for acoustic-phonon scattering is small for hole concentrations below 10^{18} cm^{-3} while it is significant for higher concentrations where other scattering mechanisms dominate. The agreement between the dashed line (with smaller effective-hole mass values) and the experimental data is excellent below the hole concentration of 10^{19} cm^{-3}, while this line is monotonically decreasing and deviates from experimental values at larger hole concentrations. At very heavily-doped conditions, we believe that the ionized impurities are strongly screened by "very heavy" holes, which is qualitatively explained by the better fit by the solid line (with larger effective-mass values). The strong nonparabolicity of the valence bands will be important in this region. We have obtained a minimum in the solid line similar to that observed for GaAs. The shallowness (or even the absence in the dashed line) of this minimum is attributed to the absence of polar phonon interaction. In polar semiconductors, the coincidence of the uncoupled LO-phonon and plasmon frequency provides a turning point, where the effects of "antiscreening" and "screening" for the LO-phonon modes take turns. In Si, there is no such point and "uncoupled" plasmon scattering plays a moderate role in the reduction of minority carrier mobilities for small hole concentrations. At higher hole concentrations, ionized impurity scattering plays a major role in determining mobility.

IV. CONCLUSION

We have proposed an alternative approach for the calculation of minority-carrier mobility in heavily-doped p-type semiconductors based on the dielectric-function formalism incorporating the broadening of collective excitations. Our calculation for p-type GaAs shows excellent agreement with recent experimental data, where we have calculated minority-carrier mobilities as a function of temperature and hole concentration. This result establishes the accuracy of the dielectric-function approach for the calculation of minority-carrier mobility. At moderate doping ($<3\times10^{18}$ cm^{-3}) in p-type GaAs, inelastic scattering due to coupled collective excitations dominates in determining minority-carrier mobilities, while ionized impurity scattering becomes increasingly important at higher doping densities. We have also successfully calculated the minority-carrier mobilities for p-type Si as a function of hole concentration by incorporating the major scattering mechanisms. Since our theory derives the damping constant parameter from experimental values of hole mobility, it should prove useful for predicting minority-carrier mobilities for other p-type semiconductors. Theoretical development in the dielectric-function formalism beyond the Born approximation is required for further understanding of electron transport in very heavily-doped semiconductor materials (e.g., $p > 10^{19}$ cm^{-3} for GaAs).

ACKNOWLEDGMENTS

The authors would like to thank Dr. G. J. Iafrate, Dr. M. A. Stroscio, and Professor B. A. Mason for helpful discussions. This work was supported in part by the Office of Naval Research and the U.S. Army Research Office.

APPENDIX A

Although the estimation of average conductivity effective mass shown in Ref. 38 is not rigorous, it is useful and easy to estimate. We will show equivalent but more explicit formulas here.

Conductivity effective mass along the $\mathbf{k}$ direction in the ith band is given by

$$m_i(E_{\mathbf{k}}) = [\hbar^2 k/(\partial E_{\mathbf{k}}/\partial k)]_i = \frac{3Q(\theta,\phi)\gamma_i^2 + 2A(\Delta - 3E_{\mathbf{k}})\gamma_i - E_{\mathbf{k}}(3E_{\mathbf{k}} - 2\Delta)}{3P(\theta,\phi)\gamma_i^2 + 2(\Delta - 3E_{\mathbf{k}})Q(\theta,\phi)\gamma_i + AE_{\mathbf{k}}(3E_{\mathbf{k}} - 2\Delta)}, \tag{A1}$$

$$Q(\theta,\phi) = -A^2 + B^2 + C^2 q(\theta,\phi), \tag{A2}$$

$$P(\theta,\phi) = (A+2B)(A-B)^2 - 3C^2(A-B)q(\theta,\phi) - 54[(B^2 + C^2/3)^{3/2} + B(B^2 + C^2/2)]p(\theta,\phi), \tag{A3}$$

$$q(\theta,\phi) = \sin^4\theta\cos^2\phi\sin^2\phi + \sin^2\theta\cos^2\theta, \tag{A4}$$

$$p(\theta,\phi) = \cos^2\theta\sin^4\theta\cos^2\phi\sin^2\phi, \tag{A5}$$

and γ_i is the root of the equation,[40]

$$H_3\gamma^3+H_2\gamma^2+H_{1\gamma}+H_0=0 , \tag{A6}$$

where

$$H_3=P(\theta,\varphi) , \tag{A7}$$

$$H_2=(\Delta-3E_k)Q(\theta,\varphi) , \tag{A8}$$

$$H_1=AE_k(3E_k-2\Delta) , \tag{A9}$$

$$H_0=E_k^2(E_k-\Delta) . \tag{A10}$$

Accordingly, we obtain a weighted average of m_i by the simple equation[38]

$$\overline{m_i}=\tfrac{1}{26}[6m_i(100)+8m_i(111)+12m_i(110)] . \tag{A11}$$

APPENDIX B

Meyer and Bartoli showed that ionized impurity scattering is intrinsically a multi-ion process and the use of a tightly screened, isolated-impurity model is unphysical.[44] Here, we have applied their formula in the Born approximation.

When $q/2k_F \ll 1$ where k_F is the wave vector at the Fermi level, the SCF dielectric function reduces to the Thomas-Fermi screening function

$$\varepsilon(q,0)\sim\varepsilon_0\left[1+\frac{q_{TF}^2}{q^2}\right] , \tag{A12}$$

where q_{TF} is the Thomas-Fermi wave vector given by

$$q_{TF}^2=\frac{4\pi e^2}{\varepsilon_0}\int_0^\infty g(E)\left[-\frac{\partial f}{\partial E}\right]dE \tag{A13}$$

and where $g(E)$ is the density of states. According to Ref. 44, q_{TF} is replaced by q_M which is obtained from the following equations:

$$q_M^2=\beta q_{TF}^2 , \tag{A14}$$

$$\beta=\frac{\int_0^{z_q}\frac{z^{1/2}}{z_q}f_0dz+\int_{z_q}^\infty z^{-1/2}f_0dz}{\int_0^\infty z^{-1/2}f_0dz} , \tag{A15}$$

$$z_q=\frac{2\pi hN_ie^2}{\varepsilon_0k_BTq_M^2} , \tag{A16}$$

$$h=1-(1+Dq_M)\exp(-Dq_M) , \tag{A17}$$

$$D=(4\pi N_i/3)^{-1/3} . \tag{A18}$$

After obtaining q_{TF} and q_M, we have replaced the SCF dielectric function with

$$\varepsilon(q,0)\rightarrow\varepsilon_0-\frac{4\pi e^2}{q^2}P(q,0)\left[\frac{q_M}{q_{TF}}\right]^2 . \tag{A19}$$

A more complete discussion and the details of the phase-shift analysis is given in the original paper.

*Present address: Ayase LSI Research Center, NKK Corporation, 2596 Yoshioka, Ayase, Kanagawa, 252 Japan.

[1]R. K. Ahrenkiel, D. J. Dunlavy, D. Greenberg, J. Schlupmann, H. C. Hamaker, and H. F. MacMillan, App. Phys. Lett. **51**, 776 (1987).
[2]B. M. Keyes, D. J. Dunlavy, R. K. Ahrenkiel, S. E. Asher, L. D. Partain, D. D. Liu, and M. S. Kuryla, J. Vac. Sci. Technol. A **8**, 2004 (1990).
[3]T. Furuta and M. Tomizawa, Appl. Phys. Lett. **56**, 824 (1990).
[4]M. L. Lovejoy, B. M. Keyes, M. E. Klausmeier-Brown, M. R. Melloch, R. K. Ahrenkiel, and M. S. Lundstron, Jpn. J. Appl. Phys. **30**, L135 (1991).
[5]C. M. Colomb, S. A. Stockman, S. Varadarajan, and G. E. Stillman, Appl. Phys. Lett. **60**, 65 (1992).
[6]M. I. Nathan, W. P. Dumke, K. Wrenner, S. Tiwari, S. L. Wright, and K. A. Jenkins, Appl. Phys. Lett. **52**, 654 (1988).
[7]S. Tiwari and S. L. Wright, Appl. Phys. Lett. **56**, 563 (1990).
[8]K. Beyzavi, K. Lee, D. M. Kim, M. I. Nathan, K. Wrenner, and S. L. Wright, Appl. Phys. Lett. **58**, 1268 (1991).
[9]R. J. Nelson, in *Gallium Arsenide and Related Compounds, 1978,* Proceedings of the Seventh International Symposium on Gallium Arsenide and Related Compounds, edited by Charles M. Wolfe, IOP Conf. Proc. No. 45 (Institute of Physics and Physical Society, London, 1979), p. 256.
[10]T. S. Lagunova, V. A. Marushchak, M. N. Stepanova, and A. N. Titkov, Fiz. Tverd. Tela (Leningrad) **19**, 118 (1985) [Sov. Phys. Semicond. **19**, 71 (1985)].
[11]H. Ito and T. Ishibashi, J. Appl. Phys. **65**, 5197 (1989).
[12]J. Dziewior and D. Silber, Appl. Phys. Lett. **35**, 170 (1979).
[13]D. D. Tang, F. F. Fang, M. Scheuermann, T. C. Chen, and G. Sai-Halasz, IEDM Tech. Dig., 1986, p. 20.
[14]S. E. Swirhun, D. E. Kane, and R. M. Swanson, IEDM Tech. Dig., 1988, p. 298.
[15]W. Walukiewicz, J. Lagowski, L. Jastrzebski, and H. C. Gatos, J. Appl. Phys. **50**, 5040 (1979).
[16]K. Sadra, C. M. Maziar, B. G. Streetman, and D. S. Tang, Appl. Phys. Lett. **53**, 2205 (1988).
[17]H. Taniyama, M. Tomizawa, T. Furuta, and A. Yoshii, J. Appl. Phys. **68**, 621 (1990).
[18]K. Saito, M. Konagai, and K. Takahashi, Jpn. J. Appl. Phys. **29**, 1900 (1990).
[19]J. R. Lowney and H. S. Bennett, J. Appl. Phys. **69**, 7102 (1991).
[20]H. S. Bennett and J. R. Lowney, J. Appl. Phys. **71**, 2285 (1992).
[21]M. V. Fischetti, Phys. Rev. B **44**, 5527 (1991).
[22]D. Pines, Phys. Rev. **92**, 626 (1953).
[23]J. M. Rorison and D. C. Herbert, J. Phys. C **19**, 3991 (1986); **19**, 6357 (1986).
[24]D. Yevic and W. Bardyszewski, Phys. Rev. B **39**, 8605 (1989).
[25]A. F. J. Levi and Y. Yefet, Appl. Phys. Lett. **51**, 42 (1987).
[26]T. Kaneto, K. W. Kim, and M. A. Littlejohn, J. Appl. Phys. **72**, 4139 (1992).
[27]D. Olego and M. Cardona, Phys. Rev. B **24**, 7217 (1981).
[28]T. Yuasa and M. Ishii, Phys. Rev. B **35**, 3962 (1987).
[29]K. Wan and J. F. Young, Phys. Rev. B **41**, 10 772 (1990).

[30]For a general discussion of RPA and its limitations, see G. D. Mahan, *Many-Particle Physics,* 2nd ed. (Plenum, New York, 1990), Chap. 5.
[31]D. L. Rode, in *Semiconductors and Semimetals,* edited by R. K. Willardson and A. C. Beer (Academic, New York, 1975), Vol. 10, Chap. 1.
[32]T. Sano and T. Kasuya, J. Phys. Soc. Jpn. **48**, 1566 (1980).
[33]D. Pines and P. Nozieres, *The Theory of Quantum Liquid* (Addison-Wesley, New York, 1989), Vol. 1.
[34]N. D. Mermin, Phys. Rev. B **1**, 2362 (1970).
[35]P. Vogl, in *Physics of Nonlinear Transport in Semiconductors,* Vol. 52 of *NATO Advanced Study Inst. Series B: Physics,* edited by D. K. Ferry, J. R. Barker, and C. Jacoboni (Plenum, New York, 1980), pp. 75–115.
[36]P. Boguslawski and J. Mycielski, J. Phys. C **10**, 2413 (1977).
[37]C. Jacoboni and L. Reggiani, Rev. Mod. Phys. **55**, 645 (1983).
[38]M. Costato, G. Gagliani, C. Jacoboni, and L. Reggiani, J. Phys. Chem. Solids **35**, 1605 (1974).
[39]C. Jacoboni and L. Reggiani, Adv. Phys. **28**, 493 (1979).
[40]F. L. Madarasz, J. E. Lang, and P. M. Hemeger, J. Appl. Phys. **52**, 4646 (1981).
[41]H. R. Chandrasekhar and A. K. Ramdas, Phys. Rev. B **21**, 1511 (1980).
[42]B. K. Ridley, *Quantum Processes in Semiconductors,* 2nd ed. (Oxford, New York, 1988).
[43]D. Chattopadhyay and H. J. Queisser, Rev. Mod. Phys. **53**, 745 (1981).
[44]J. R. Meyer and F. J. Bartoli, Phys. Rev. B **36**, 5989 (1987).
[45]E. J. Moore, Phys. Rev. **160**, 618 (1967).